Development 140, 1220-1230 (2013) doi:10.1242/dev.089615

Smad4-Irf6 genetic interaction and TGFβ-mediated IRF6 signaling cascade are crucial for palatal fusion in mice

Jun-ichi Iwata[1], Akiko Suzuki[1], Richard C. Pelikan[1], Thach-Vu Ho[1], Pedro A. Sanchez-Lara[2,3], Mark Urata[1,4], Michael J. Dixon[5] and Yang Chai[1,*]

SUMMARY

Cleft palate is one of the most common human birth defects and is associated with multiple genetic and environmental risk factors. Although mutations in the genes encoding transforming growth factor beta (TGFβ) signaling molecules and interferon regulatory factor 6 (Irf6) have been identified as genetic risk factors for cleft palate, little is known about the relationship between TGFβ signaling and IRF6 activity during palate formation. Here, we show that TGFβ signaling regulates expression of *Irf6* and the fate of the medial edge epithelium (MEE) during palatal fusion in mice. Haploinsufficiency of *Irf6* in mice with basal epithelial-specific deletion of the TGFβ signaling mediator *Smad4* (*Smad4$^{fl/fl}$;K14-Cre;Irf6$^{+/R84C}$*) results in compromised p21 expression and MEE persistence, similar to observations in *Tgfbr2$^{fl/fl}$;K14-Cre* mice, although the secondary palate of *Irf6$^{+/R84C}$* and *Smad4$^{fl/fl}$;K14-Cre* mice form normally. Furthermore, *Smad4$^{fl/fl}$;K14-Cre;Irf6$^{+/R84C}$* mice show extra digits that are consistent with abnormal toe and nail phenotypes in individuals with Van der Woude and popliteal pterygium syndromes, suggesting that the TGFβ/SMAD4/IRF6 signaling cascade might be a well-conserved mechanism in regulating multiple organogenesis. Strikingly, overexpression of *Irf6* rescued p21 expression and MEE degeneration in *Tgfbr2$^{fl/fl}$;K14-Cre* mice. Thus, IRF6 and SMAD4 synergistically regulate the fate of the MEE, and TGFβ-mediated *Irf6* activity is responsible for MEE degeneration during palatal fusion in mice.

KEY WORDS: TGFβ, IRF6, Palatal fusion, Mouse

INTRODUCTION

Cleft palate is a serious and common craniofacial birth defect affecting millions of people worldwide (Mossey et al., 2009; Wong and Hagg, 2004). Cleft palate has ethnic and geographic variations in prevalence, and it affects feeding, swallowing, speech, hearing, middle-ear ventilation, respiration and appearance (Iwata et al., 2011). Studies in mouse models and genetic screening in humans have implicated several factors in syndromic cleft palate, such as *IRF6* mutation in Van der Woude syndrome (VWS) and popliteal pterygium syndrome (PPS), *SMAD4* mutation in juvenile polyposis syndrome, and *TGFBR1* or *TGFBR2* mutation in Loeys-Dietz syndrome (previously called Marfan syndrome type II). Mutations in *TGFB3*, *IRF6*, *CYP* (cytochrome P450), *MSX1* and *TBX10* have also been associated with non-syndromic cleft lip with or without cleft palate (NSCL/P) (Iwata et al., 2011). In addition, polymorphic variants associated with NSCL/P within human chromosomes 1q32 (*IRF6*), 1p22 (*ABCA4*), 8q24.21, 10q25 (*VAX1*), 17q22 and 20q12 (*MAFB*) have been identified by genome-wide association studies (Dixon et al., 2011). Thus, mutations in *IRF6*, *SMAD4* and *TGFBR2* confer a significant attributable risk for cleft palate.

TGFβ signaling is one of the major signaling cascades crucial for craniofacial development (Iwata et al., 2011). Epithelial-specific deletion of *Tgfbr2* (*Tgfbr2$^{fl/fl}$;K14-Cre*) in mice results in persistence of the medial edge epithelium (MEE) and submucous cleft palate (Xu et al., 2006). TGFβ transmits signals through a membrane receptor serine/threonine kinase complex that phosphorylates SMAD2 and SMAD3, followed by the formation of transcriptional complexes with SMAD4 and translocation into the nucleus (Massagué, 2012; Ross and Hill, 2008; Schmierer and Hill, 2007; Shi and Massagué, 2003). TGFβ also activates SMAD-independent signaling cascades, including mitogen-activated protein kinase (MAPK) pathways, such as p38 MAPK (MAPK14 – Mouse Genome Informatics), under certain physiological and pathological conditions (Kang et al., 2009; Xu et al., 2008; Zhang, 2009). Studies using SMAD4-deficient cells, or dominant-negative SMADs, support the possibility that MAPK activation is independent of SMADs (Chen et al., 1998; Giehl et al., 2000; Hocevar et al., 1999; Hu et al., 1999). p38 MAPK activation by TGFβ is accompanied by SMAD-independent, TRAF6 and TAK1 (MAP3K7 – Mouse Genome Informatics) phosphorylation (Iwata et al., 2012; Sorrentino et al., 2008; Yamashita et al., 2008). The balance between direct activation of SMADs and MAPK pathways often defines cellular responses to TGFβ.

IRF6 belongs to a family of transcription factors that share a highly conserved, helix-turn-helix, DNA-binding domain and a less conserved, protein-binding domain. Among the genes that have been associated with NSCL/P, *IRF6* has been implicated in the largest percentage of cases (Koillinen et al., 2005; Srichomthong et al., 2005). Mutation of *IRF6* can lead to the autosomal-dominant conditions VWS and PPS, which are characterized by oral clefting and lower lip pits (Kondo et al., 2002; Moretti et al., 2010). VWS and PPS are allelic variants of the same condition caused by different mutations of the same gene. PPS includes all the features of VWS, plus popliteal pterygia, syngnathia, distinct toe and nail abnormality, syndactyly and genito-urinary malformations. An arginine 84 to cysteine (R84C) mutation in *IRF6* is the most common mutation found in patients with PPS (Richardson et al., 2006). Although the function of the R84C mutation is still largely

[1]Center for Craniofacial Molecular Biology, Ostrow School of Dentistry, University of Southern California, Los Angeles, CA 90033, USA. [2]Department of Pediatrics, Keck School of Medicine, University of Southern California, Los Angeles, CA 90033, USA. [3]Division of Medical Genetics, Children's Hospital Los Angeles, Los Angeles, CA 90033, USA. [4]Division of Plastic Surgery, Children's Hospital Los Angeles, Los Angeles, CA 90033, USA. [5]Faculty of Life Sciences and Dental School, University of Manchester, Manchester, UK.

*Author for correspondence (ychai@usc.edu)

Accepted 31 December 2012

unknown, recent studies have demonstrated that it results in loss of DNA binding (Kondo et al., 2002; Little et al., 2009). The primary defect in *Irf6*-deficient mice is in keratinocyte differentiation and proliferation. Homozygous $Irf6^{gt1/gt1}$ (null) embryos exhibit abnormal skin, limb and craniofacial morphogenesis, including cleft palate (Ingraham et al., 2006). Mice homozygous for $Irf6^{R84C}$, which is an R84C knock-in resulting in expression of mutant IRF6 protein, exhibit a severe intraoral epithelial adhesion caused by a failure of terminal differentiation similar to that in homozygous $Irf6^{gt1/gt1}$ (null) embryos (Ingraham et al., 2006; Richardson et al., 2006).

Despite the established roles of TGFβ signaling and IRF6 activity during palate formation, the interaction between TGFβ signaling and IRF6 activity is poorly understood. In this study, we investigate the interaction between TGFβ signaling and IRF6 activity. We demonstrate that *Irf6* and *Smad4* interact genetically, and that TGFβ-mediated *Irf6* expression is crucial for p21 (CDKN1A – Mouse Genome Informatics) expression and fate determination of the MEE cells during palatal fusion.

MATERIALS AND METHODS

Animals

To generate $Smad4^{fl/fl}$;*K14-Cre*;$Irf6^{+/R84C}$ mice, we mated $Smad4^{fl/+}$;*K14-Cre*;$Irf6^{+/R84C}$ with $Smad4^{fl/fl}$ mice. To generate $Tgfbr2^{fl/fl}$;*K14-Cre* mice, we mated $Tgfbr2^{fl/+}$;*K14-Cre* with $Tgfbr2^{fl/fl}$ mice. Genotyping was performed using PCR primers as previously described (Ito et al., 2003; Richardson et al., 2009; Xu et al., 2008; Xu et al., 2006). Human keratin 14 (K14; KRT14 – Human Gene Nomenclature Database) promoter-driven *Irf6*-encoding transgene was prepared as follows: an *Eco*RI-*Hin*dIII blunted fragment (7.3 kb) encoding mouse *Irf6* was subcloned into the *Bam*HI blunted sites of the pGEM 3Z-K14 vector to produce pG3ZK14-*Irf6*, resulting in a construct containing the *K14* promoter (2.1 kb), the β-globin intron (736 bp), the coding sequence for *Irf6* (4.1 kb) and the K14 polyadenylation signal (500 bp). The *Eco*RI-*Hin*dIII fragment was isolated free of vector sequence by preparative gel electrophoresis. DNA was further purified using an Elutip column (Schleicher and Schuell, Dessell, Germany) and microinjected in the pronuclei of fertilized oocytes (Jackson/B6D2F F1) following standard procedures. Transgenic founder mice were identified by PCR analysis. PCR amplification of tail genomic DNAs (0.5-1 μg) was performed on a thermal cycler, with 35 cycles consisting of 94°C, 62°C and 72°C for 1 minute each. An aliquot (15 μl) of each reaction was resolved in a 1% agarose gel, and amplified fragments were visualized by ethidium bromide staining. The PCR primers used were 5′-TCAGGAGC-AGGTGCACAAGAGTT-3′ and 5′-ACTCGCATCCCTTTCCAATTTAC-3′. To generate $Tgfbr2^{fl/fl}$;*K14-Cre*;$Irf6^{Tg}$ mice, we mated $Tgfbr2^{fl/+}$;*K14-Cre*;$Irf6^{Tg}$ with $Tgfbr2^{fl/fl}$ mice. Genotyping was performed using PCR primers as previously described (Ito et al., 2003; Xu et al., 2008; Xu et al., 2006). All mouse experiments were conducted in accordance with protocols approved by the Department of Animal Resources and the Institutional Animal Care and Use Committee of the University of Southern California.

Comparative analysis of transcription factor-binding sites

Genomic sequences of the entire human and murine *IRF6* (RefSeq accession NM_006147.3/hg19 and NM_016851.2/mm10), *p63* (RefSeq accession NM_001114980/hg19 and NM_011641.2/mm10) and *CDKN1A/p21* (RefSeq accession NM_000389.4/hg19 and NM_007669.4/mm10) genes were obtained from the University of California, Santa Cruz (UCSC) genome browser, including 2.5 kb upstream and 2.5 kb downstream of the respective transcription start sites (TSSs), based on mouse genome Build 38. These sequences were mapped to seven additional mammalian genomes [chimpanzee (Build 2.1.4), orangutan (Build 2.0.2), rhesus macaque (Build 1.0), human (Build 19), rat (Build 5), dog (Build 3.1) and horse (Build equCab2)] using the BLAT tool. Multiple alignments for these sequences were obtained using the ClustalW2 tool with default parameters and settings (Larkin et al., 2007). To account for uncertainty in the quality of the horse and dog draft genome sequences, sequence alignments with and without information from these species were performed. Transcription factor-binding motifs relevant to SMAD, p63 (TRP63 – Mouse Genome Informatics) and p38 MAPK pathway elements were searched within and proximal to these genes (i.e. 2.5 kb upstream and 2.5 kb downstream of the mouse TSS for each gene). The recognition sequences searched for SMAD binding were 5′-GTCT-3′, 5′-AGAC-3′ and 5′-GTCTAGAC-3′ (Denissova et al., 2000; Zawel et al., 1998) and for MEF2 family member binding was 5′-YTAWWWWTAR-3′ (Black and Olson, 1998). In addition, we evaluated the following potential p63 recognition sites: the canonical p53 family 20-base recognition sequence formed from duplicates of the half-site recognition sequence 5′-RRRCWWGYYY-3′ separated by any combination of 0 to 13 bases (Cai et al., 2012; el-Deiry et al., 1992) and the p63-preferential recognition sequence 5′-RRRCRWGYYYRRRCWYGYYY-3′ (Perez et al., 2007). To account for the possibility of degenerate p53 family member-binding sites, we used the p53scan and p63scan algorithms with default options (Kouwenhoven et al., 2010), which allow the consensus half-site to vary slightly in composition. Finally, we also searched for the eight-base recognition sequence 5′-AANNGAAA-3′ for the DNA-binding domains of IRF family members (Fujii et al., 1999) and the more specific ten-base recognition sequence 5′-AACCGAAACY-3′ for the IRF6 DNA-binding domain (Little et al., 2009).

Promoter-proximal search of p53-family responsive elements

The aforementioned consensus recognition sequences of p53 family members (see previous section) were used to search the murine and human *p21* genomic sequences for putative p53 and p63 recognition sites proximal to the promoter. Genomic sequences were obtained from the UCSC genome browser, spanning a 5-kb window centered around the transcription start site of each *p21* RefSeq transcript variant in the murine genome (build mm10, 2 transcript variants) and human genome (build hg19, 4 transcript variants).

Chromatin immunoprecipitation (ChIP) assay

Back skin was dissected from embryonic day (E) 13.5 C57B6/J mouse embryos in PBS. For the separation of skin epithelium from mesenchyme, the explants were incubated in 0.25% dispase (Invitrogen) for 30 minutes at 37°C. The epithelium was further dissociated in a 0.25% trypsin-EDTA solution for 10 minutes at 37°C, fixed with 1% formaldehyde for 15 minutes at room temperature and lysed in cell lysing buffer (Cell Signaling Technology) with a cocktail of proteinase inhibitors (Ultra Complete Mini, Roche). After pre-clearing treatment, cell extracts were incubated with anti-SMAD4, anti-MEF2 (Cell Signaling Technology), anti-p63 or IgG control (Santa Cruz Biotechnology) antibodies for two hours according to the manufacturer's protocol (Cell Signaling Technology). We assayed for the presence of putative target sites in the immune complexes by PCR using primers amplifying the following genomic regions: mouse *Irf6* promoter SMAD-binding site (BS) 1, 5′-GCAGGTCCTCGTGCTAGTTC-3′and 5′-CTGCCTCTTCGTCACCCTAC-3′; mouse *Irf6* promoter SMAD BS 2, 5′-GGAAGCTATTCTGGGCCTCT-3′ and 5′-GCAGCTTTATTTGGGT-GCTT-3′; mouse *Irf6* promoter SMAD BS 3, 5′-TGTGCT-ATTAGCCCCAACCT-3′ and 5′-TGTAGGGGGTTGAGTGTGGT-3′; mouse *Irf6* promoter MEF2 BS, 5′-CGATCACAACACCAATCTGC-3′ and 5′-GACAGGCTGTGCACTCTTGA-3′, mouse *p21* promoter p63 BS 1, 5′-CTTAGCGCAGAGCGGTTC-3′ and 5′-ACCTCCTCGCCTGT-CCTCTA-3′; and mouse *p21* promoter p63 BS 2, 5′-TGGTCT-CCATCGGAATAGGT-3′ and 5′-TGTTTGCCTAACTTGCTGGA-3′. Positions of PCR fragments correspond to National Center for Biotechnology Information (NCBI) mouse genome Build 33.1.

Histological examination

Hematoxylin and Eosin (H&E), immunohistochemical and 5-bromo-2′-deoxyuridine (BrdU) staining were performed as described previously (Iwata et al., 2012; Iwata et al., 2010). Antibodies used for immunohistochemistry were rabbit polyclonal antibodies against p21 (Santa Cruz Biotechnology), IRF6 (Aviva Systems Biology), phosphorylated histone H3 (Millipore) and Lex/SSEA1 (FUT4 – Mouse Genome Informatics) (Cell Signaling Technology), and mouse monoclonal antibody against p63 (Santa Cruz Biotechnology). Fluorescence images were obtained using a fluorescence microscope (Model IX71, Olympus).

Immunoblot analysis

Immunoblots were performed as described previously (Iwata et al., 2006; Iwata et al., 2010). Antibodies used for immunoblotting were rabbit polyclonal antibodies against IRF6 (Aviva Systems Biology) and p21 (Abcam), and mouse monoclonal antibodies against p63 (Santa Cruz Biotechnology) and GAPDH (Chemicon).

Palatal shelf organ culture

Timed pregnant mice were sacrificed at E13.5. Genotyping was carried out as described above. The palatal shelves were microdissected and cultured in serum-free chemically defined medium as previously described (Ito et al., 2003; Xu et al., 2008). After 48 or 72 hours in culture, palates were harvested, fixed in 4% paraformaldehyde in 0.1 M phosphate buffer (pH 7.4), and processed. For p63 experiments, palatal shelves were transfected with small interfering RNA (siRNA) duplexes (500 nM) for *p63* or control (Santa Cruz Biotechnology). The 500 nM siRNA solutions were prepared by diluting a siRNA stock (10 μM) in BGJb medium containing Oligofectamine (0.3%) (Invitrogen). The siRNA mixture in transfection medium was changed every 24 hours and incubated with palatal shelves up to 72 hours after siRNA treatment at 37°C in a CO_2 incubator. For experiments with p21, palatal shelves were transfected with a GFP-tagged *p21* overexpression or control vector (Origene). The 2-μg *p21* transfection solutions were prepared in BGJb medium containing Lipofectamine LTX and PLUS reagents (Invitrogen) according to the manufacturer's protocol. The *p21* transfection mixture was changed every 24 hours and incubated with palatal shelves up to 72 hours after transfection at 37°C in a CO_2 incubator. All experiments were performed with at least five samples.

Cell culture

Primary mouse keratinocytes were isolated from newborn mice and cultured in dermal cell basal medium (ATCC) supplemented with the Keratinocyte Growth Kit (ATCC). Primary mouse keratinocytes (2×10^6 cells) were plated in a 60-mm cell culture dish until the cells reached 60-80% confluence. *Tgfbr2* and *Irf6* siRNA duplexes were purchased from Santa Cruz Biotechnology. siRNA mixture in transfection medium was incubated with cells for 7 hours at 37°C in a CO_2 incubator, as described previously (Iwata et al., 2010).

Quantitative reverse transcription PCR (RT-PCR)

Total RNA was isolated from dissected mouse MEE at E14.5 with the QIAshredder and RNeasy Micro Extraction Kit (QIAGEN), as described previously (Iwata et al., 2010). The following PCR primers were used: *Irf6*, 5′-AGGGCTCTGTCATTAATCCAG-3′ and 5′-TGATTCGGGGCT-GCAGTTTC-3′; *p21* (*Cdkn1a*), 5′-AGCCTGAAGACTGTGATGGG-3′ and 5′-AAAGTTCCACCGTTCTCGG-3′; *ΔNp63*, 5′-CAAAACCC-TGGAAGCAGAAA-3′ and 5′-GAGGAGCCGTTCTGAATCTG-3′; and *Gapdh*, 5′-AACTTTGGCATTGTGGAAGG-3′ and 5′-ACACATTG-GGGGTAGGAACA-3′.

Scanning electron microscopic (SEM) analysis

Samples were fixed with a modified Karnovsky fixative solution [2% paraformaldehyde and 2.5% glutaraldehyde in 0.067 M cacodylate buffer (pH 7.4)] for two days. After dehydration through a graded ethanol series, samples were critical-point dried in a Balzer Union apparatus (FL-9496), ion-sputtered with platinum-palladium (10-15 nm), and observed in JEOL JSM-6390 low vacuum scanning electron microscope (JEOL USA, MA, USA) at a low accelerating voltage of 10 kV.

Whole-mount skeletal staining and micro-CT analysis

The three-dimensional architecture of the skeleton was examined using a modified whole-mount Alcian Blue-Alizarin Red S staining protocol as previously described (Ito et al., 2003; Iwata et al., 2012). Micro-CT analysis was performed using SCANCO μCT 50 (nanoCT) at the University of

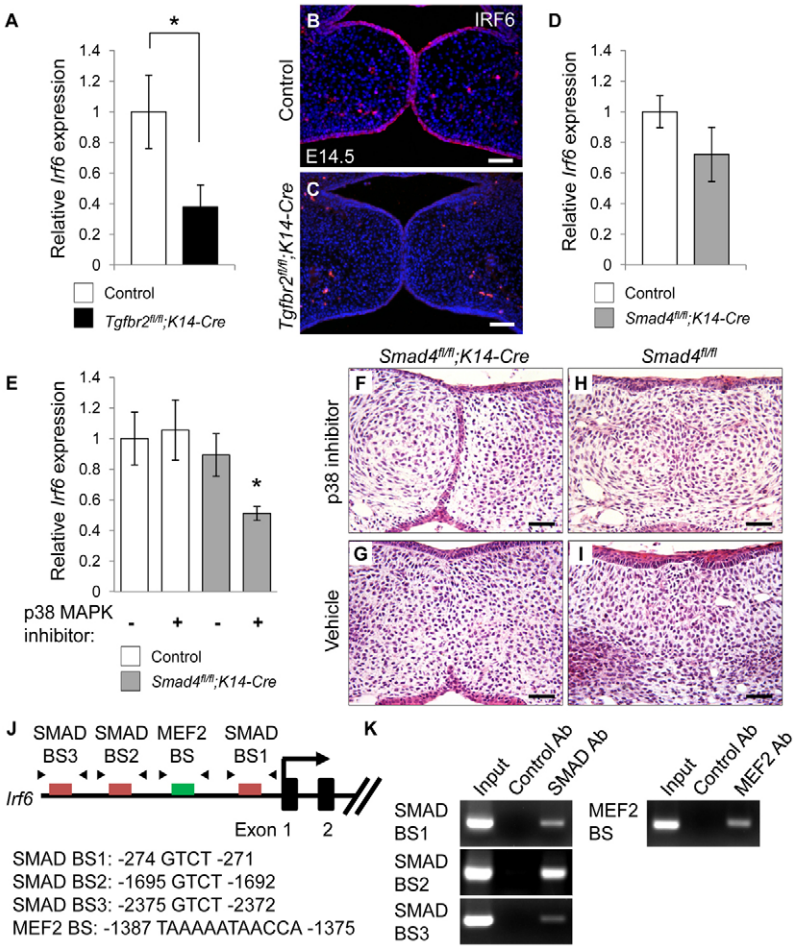

Fig. 1. Decreased IRF6 expression in the MEE of *Tgfbr2$^{fl/fl}$;K14-Cre* mice. (**A**) Quantitative RT-PCR analyses of *Irf6* expression in the palates of *Tgfbr2$^{fl/fl}$* (control, *n*=6) and *Tgfbr2$^{fl/fl}$;K14-Cre* (*n*=6) mice at E14.5. (**B**,**C**) Immunohistochemical analyses of IRF6 expression (red) in the palates of *Tgfbr2$^{fl/fl}$* control (B) and *Tgfbr2$^{fl/fl}$;K14-Cre* (C) mice at E14.5. Nuclei were counterstained with DAPI (blue). (**D**) Quantitative RT-PCR analyses of *Irf6* expression in the palates of *Smad4$^{fl/fl}$* (control, *n*=6) and *Smad4$^{fl/fl}$;K14-Cre* (*n*=6) mice at E14.5. (**E**) Quantitative RT-PCR analyses of *Irf6* expression in palate explants from *Smad4$^{fl/fl}$* (control) and *Smad4$^{fl/fl}$;K14-Cre* mice treated with p38 MAPK inhibitor (+) or vehicle (–) for 48 hours. *n*=3 per group. (**F-I**) H&E staining of palate explants from *Smad4$^{fl/fl}$;K14-Cre* and *Smad4$^{fl/fl}$* (control) mice treated with p38 MAPK inhibitor (F,H) or vehicle control (G,I) for 72 hours. *n*=5 per group. (**J**) Schematic of the upstream region of the mouse *Irf6* gene (not to scale), showing locations of putative SMAD-binding (red) or MEF2-binding (green) sites tested in ChIP assays. Putative SMAD- and MEF2-binding sequences are shown below. Arrowheads indicate the position of primers used in ChIP analysis. (**K**) ChIP analysis of DNA fragments immunoprecipitated with a SMAD4-specific or MEF2-specific antibody or with an isotype-specific control antibody. Immunoprecipitates were PCR amplified with primers flanking the putative SMAD-binding or MEF2-binding region. Input lane shows PCR amplification of the sonicated chromatin before immunoprecipitation. Ab, antibody; BS, binding site. Error bars represent s.d. *P<0.05. Scale bars: 50 μm.

Southern California Molecular Imaging Center. The data were collected at a resolution of 10 μm. The reconstruction was performed using AVIZO 7.0 (Visualization Sciences Group).

Statistical analysis

A two-tailed Student's *t*-test was applied for statistical analysis. For all graphs, data are represented as mean±s.d. A *P*-value of less than 0.05 was considered statistically significant.

RESULTS

TGFβ signaling in the MEE regulates *Irf6* expression during palatal fusion

Loss of TGFβ signaling in the basal epithelium in mice (*Tgfbr2*$^{fl/fl}$*;K14-Cre*) results in diminished *Irf6* expression and failure of apoptosis in MEE cells, followed by MEE persistence, suggesting that TGFβ-mediated *Irf6* expression might play a role in degeneration of the MEE (Xu et al., 2006). The MEE is composed of a basal columnar cell layer covered by flat cells that constitute the periderm (Cuervo and Covarrubias, 2004). *Irf6* is expressed in the periderm at E13.5, and *Irf6* expression shows an obvious and consistent transition from the periderm to regions of the basal epithelial layer at E14.5 (Fakhouri et al., 2012). Expression of *Irf6* mRNA (Fig. 1A) and protein (Fig. 1B,C) was decreased in *Tgfbr2*$^{fl/fl}$*;K14-Cre* mice at E14.5. We found no defect in the periderm of *Tgfbr2*$^{fl/fl}$*;K14-Cre* mice during palatal fusion (supplementary material Fig. S1). To test whether *Irf6* expression is regulated by a SMAD-dependent pathway, we analyzed gene expression of *Irf6* in *Smad4*$^{fl/fl}$*;K14-Cre* mice. *Irf6* expression was not significantly changed in *Smad4*$^{fl/fl}$*;K14-Cre* mice (Fig. 1D), suggesting that SMAD4-independent TGFβ signaling might be involved in the induction of *Irf6* in MEE cells during palatogenesis. Because SMAD4 and p38 MAPK are functionally redundant in regulating the MEE disappearance (Xu et al., 2008), we performed *ex vivo* organ culture of E13.5 palatal shelf explants from *Smad4*$^{fl/fl}$*;K14-Cre* and *Smad4*$^{fl/fl}$ control mice with p38 MAPK inhibitor or with vehicle as control. We found that p38 MAPK inhibitors blocked both *Irf6* expression (Fig. 1E) and MEE disappearance (Fig. 1F) in *Smad4*$^{fl/fl}$*;K14-Cre* palates but did not affect *Irf6* expression (Fig. 1E) or MEE disappearance (Fig. 1H) in control samples, indicating that SMAD and p38 MAPK activation are functionally redundant in regulating *Irf6* expression and MEE disappearance.

Next, we analyzed the sequence of the mouse *Irf6* gene (including 2.5 kb upstream and 2.5 kb downstream of the transcription start site). The mouse *Irf6* genomic region has 43 potential SMAD recognition sites (three of which are conserved in at least six mammals) (Fig. 1J; supplementary material Table S1). The MEF2 transcription factor is regulated by the p38 MAPK pathway (Han and Molkentin, 2000; Toro et al., 2004). We found a potential MEF2 recognition site in the *Irf6* genomic region (Fig. 1J). We performed chromatin immunoprecipitation (ChIP) assays to test whether SMAD and MEF2 could bind to the promoter region of *Irf6*. Binding sites for SMAD (SMAD binding site 1: −274 bp to −271 bp; site 2: −1695 bp to −1692 bp; site 3: −2375 bp to −2372 bp) and MEF2 (MEF2 binding site: −1387 bp to −1375 bp) immunoprecipitated with SMAD4 or MEF2 antibodies, but not with control antibody (Fig. 1K). Taken together, our results suggest that *Irf6* gene expression is regulated by both SMAD and p38 MAPK pathways.

Next, we investigated the functional significance of *Irf6* in regulating the disappearance of MEE cells during palatal fusion. Because homozygous mutation of *Irf6* results in severe intraoral epithelial adhesion, it is not known whether *Irf6* is crucial for palatal fusion (Ingraham et al., 2006; Richardson et al., 2006). To investigate the fate of the MEE in *Irf6*$^{R84C/R84C}$ mice, we used the *ex vivo* organ culture system. E13.5 wild-type control (*n*=17) and *Irf6*$^{+/R84C}$ (*n*=39) palate explants fused and the MEE disappeared following two days of culture (Fig. 2A,B). By contrast, *Irf6*$^{R84C/R84C}$ mutant (*n*=19) palatal shelves failed to fuse (Fig. 2C) and the MEE persisted with continuous cell proliferation (Fig. 2D-F) and compromised cell death (Fig. 2G-I) following two days of culture with complete phenotype penetrance. We quantified the increased cell proliferation as well as decreased apoptosis in *Irf6*$^{R84C/R84C}$ MEE cells compared with wild-type littermate control and *Irf6*$^{+/R84C}$ MEE cells during palatal fusion (Fig. 2J,K). The MEE in control and *Irf6*$^{+/R84C}$ explants disappeared completely following three days in culture; however, the MEE persisted in *Irf6*$^{R84C/R84C}$ explants (supplementary material Fig. S2). These data indicate that IRF6 is crucial for MEE disappearance during palatal fusion.

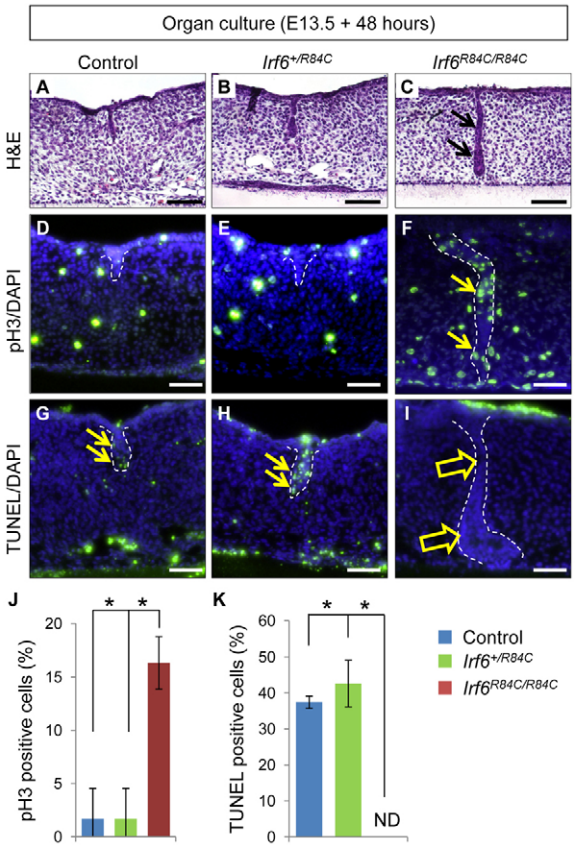

Fig. 2. *Irf6* is crucial for MEE disappearance during palate formation. (**A-C**) H&E staining of sections of control (A), *Irf6*$^{+/R84C}$ (B) and *Irf6*$^{R84C/R84C}$ (C) palates after culture for 48 hours. Arrows indicate MEE persistence. (**D-F**) Phosphorylated histone H3 (pH3) staining of sections of control (D), *Irf6*$^{+/R84C}$ (E) and *Irf6*$^{R84C/R84C}$ (F) palates after culture for 48 hours. Arrows indicate pH3-positive cells (green) in the MEE. Dashed lines outline MEE cells. Nuclei were counterstained with DAPI (blue). (**G-I**) TUNEL staining of sections of control (G), *Irf6*$^{+/R84C}$ (H) and *Irf6*$^{R84C/R84C}$ (I) palates after culture for 48 hours. Arrows indicate TUNEL-positive cells (green) in the MEE. Dashed lines outline MEE cells. Nuclei were counterstained with DAPI (blue). (**J**) Quantification of the number of phosphorylated histone H3 (pH3)-positive nuclei in the MEE in control (*n*=17), *Irf6*$^{+/R84C}$ (*n*=39) and *Irf6*$^{R84C/R84C}$ (*n*=19) palates. (**K**) Quantification of the number of TUNEL-labeled nuclei in the MEE in control (*n*=17), *Irf6*$^{+/R84C}$ (*n*=39) and *Irf6*$^{R84C/R84C}$ (*n*=19) palates. Error bars represent s.d. **P*<0.01. ND, not detected. Scale bars: 50 μm.

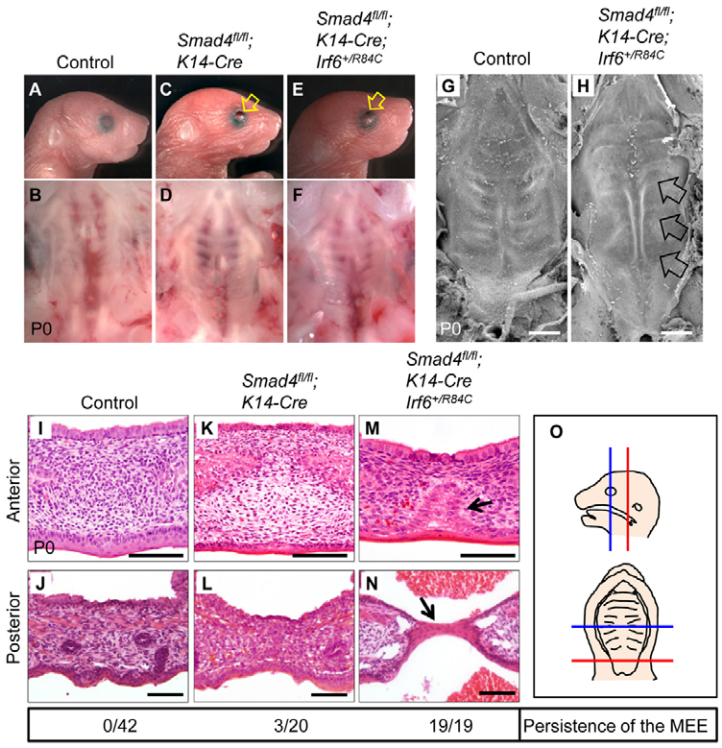

Fig. 3. A haploinsufficiency of *Irf6* in *Smad4$^{fl/fl}$;K14-Cre* mice causes submucous cleft palate. (**A-F**) Morphologies of newborn control (A,B), *Smad4$^{fl/fl}$;K14-Cre* (C,D) and *Smad4$^{fl/fl}$;K14-Cre;Irf6$^{+/R84C}$* (E,F) mice. Lower panels (B,D,F) show macroscopic appearance of palates at newborn stage. Arrows indicate open eyes. (**G**,**H**) SEM analysis of newborn control (G) and *Smad4$^{fl/fl}$;K14-Cre;Irf6$^{+/R84C}$* (H) mice. Arrows indicate lack of rugae formation. (**I-N**) H&E staining of sections of newborn *Smad4$^{fl/fl}$* control (I,J; *n*=42), *Smad4$^{fl/fl}$;K14-Cre* (K,L; *n*=20) and *Smad4$^{fl/fl}$;K14-Cre;Irf6$^{+/R84C}$* (M,N; *n*=19) mice. Arrows indicate MEE persistence. (**O**) Schematics showing the position from which the sections shown in I-N were taken. Blue lines indicate the anterior region of the palate (hard palate; I,K,M), and red lines indicate the posterior region of the palate (soft palate; J,L,N). The MEE was scored for persistence in I-N (shown below). Scale bars: 500 μm in G,H; 100 μm in I-N.

Genetic interaction between *Smad4* and *Irf6* during palatal fusion

We hypothesized that haploinsufficiency of *Irf6* in a *Smad4* mutant background would cause an additional reduction of IRF6 activity and result in cleft palate. To investigate a possible genetic interaction between *Irf6* and *Smad4*, we generated *Smad4$^{fl/fl}$;K14-Cre;Irf6$^{+/R84C}$* mice. *Smad4$^{fl/fl}$;K14-*Cre mice have normal palates although they have open eyes, short fingers, and nail abnormalities (*n*=17/20) (Fig. 3; supplementary material Fig. S3). Interestingly, *Smad4$^{fl/fl}$;K14-Cre;Irf6$^{+/R84C}$* mice exhibited extra digits with complete phenotype

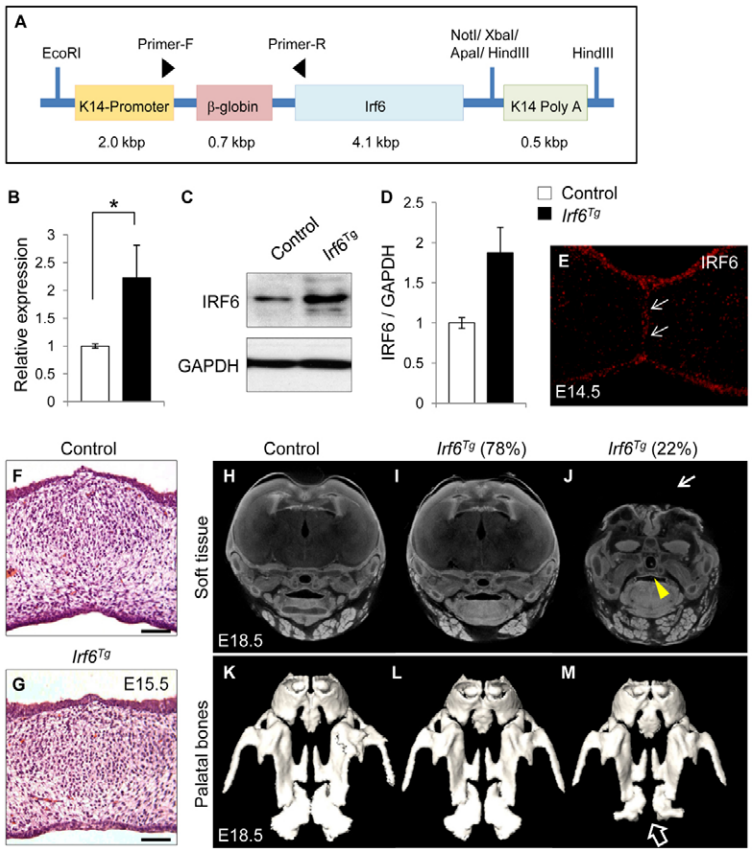

Fig. 4. Generation of *K14-Irf6* transgenic mice. (**A**) Construct used to generate *K14-Irf6* transgenic mice. (**B**) Quantitative RT-PCR analyses of *Irf6* in the palates of control and *K14-Irf6^{Tg}* mice at E14.5. *n*=6 per genotype. **P*<0.05. (**C**) Immunoblotting analysis of IRF6 in the MEE of control and *K14-Irf6^{Tg}* mice. GAPDH was used as a loading control. (**D**) Bar graph shows the ratio of IRF6 per GAPDH following quantitative densitometry analysis of immunoblotting data. Three samples were analyzed. (**E**) Immunohistochemical analysis of IRF6 in the palate of E14.5 *K14-Irf6^{Tg}* mice. Arrows indicate IRF6 expression in the MEE. (**F**,**G**) H&E staining of littermate control (F) and *K14-Irf6* transgenic (*Irf6^{Tg}*; G) mice at E15.5. Scale bars: 50 μm. (**H-J**) MicroCT analysis of the soft tissues of E18.5 control (H) and *K14-Irf6^{Tg}* (I,J) mice. Seventy-eight percent of *K14-Irf6^{Tg}* mice exhibit apparently normal development (I), and 22% exhibit severe craniofacial deformities (J). Arrowhead indicates palatal fusion in the *K14-Irf6^{Tg}* mice with severe craniofacial deformities. Arrow indicates calvarial defect in the *K14-Irf6^{Tg}* mice. (**K-M**) MicroCT analysis of the hard tissue of E18.5 control mice (K) and *K14-Irf6^{Tg}* mice with normal development (L) or with severe craniofacial deformities (M). Arrow indicates hypoplasia of the palatine bones in *K14-Irf6^{Tg}* mice with severe craniofacial deformities. Error bars represent s.d.

penetrance (*n*=19/19) (supplementary material Fig. S3). Thus, *Smad4*$^{fl/fl}$*;K14-Cre;Irf6*$^{+/R84C}$ mice have a more severe phenotype than do *Smad4*$^{fl/fl}$*;K14*-Cre mice, suggesting that IRF6 and SMAD4 function synergistically in regulating embryogenesis. In addition, the extra digits in *Smad4*$^{fl/fl}$*;K14-Cre;Irf6*$^{+/R84C}$ mice are consistent with the abnormal toe and nail phenotype in individuals with VWS and PPS. Because some individuals with VWS and PPS have cleft palate, we investigated the palate in *Smad4*$^{fl/fl}$*;K14-Cre;Irf6*$^{+/R84C}$ mice in detail by scanning electron microscopy (SEM), and detected compromised rugae formation (Fig. 3G,H). By histological analysis, we found that all *Smad4*$^{fl/fl}$*;K14-Cre;Irf6*$^{+/R84C}$ mice exhibited submucous cleft palate at birth with persistence of the MEE (*n*=19/19) and in some cases a stretched epithelial bridge (*n*=6/19) (Fig. 3I-O). Taken together, our findings suggest that a genetic interaction between *Smad4* and *Irf6* is responsible for MEE disappearance during palatal fusion.

Rescue of palatal fusion in *Tgfbr2*$^{fl/fl}$*;K14-Cre* mice by overexpression of *Irf6*

To test whether *Irf6* expression level controls MEE cell fate, we generated K14-driven *Irf6* transgenic (*K14-Irf6*^{Tg}) mice to overexpress *Irf6* in MEE cells (Fig. 4A). Most *K14-Irf6*^{Tg} mice were born healthy and fertile without any noticeable pathological phenotype up to the age of one year (*n*=114/146) (supplementary material Table S2). We analyzed *Irf6* gene expression level by quantitative RT-PCR and found that there is a significant increase in *Irf6* expression (2.2-fold) in the MEE of *K14-Irf6*^{Tg} mice compared with control (Fig. 4B). Moreover, we confirmed the overexpression of IRF6 protein in the MEE by immunoblotting (Fig. 4C,D) and immunostaining (Fig. 4E) at E14.5. Approximately 22% of *Irf6* transgenic mice (*n*=32/146) exhibited absence of the calvaria and an open eye phenotype and died within one day of birth (supplementary material Table S2 and Fig. S4). Although these *Irf6* transgenic mice exhibited severe calvarial defects and hypoplasia of the palatine bones (Fig. 4J,M), their palatal shelves fused normally without obvious cleft palate or persistence of the MEE (Fig. 4J). Palatal fusion appeared to be unaffected in all *K14-Irf6*^{Tg} mice (*n*=146) (Fig. 4F-M; supplementary material Table S2).

Next, we generated *Tgfbr2*$^{fl/fl}$*;K14-Cre;Irf6*^{Tg} mice to restore *Irf6* gene expression in *Tgfbr2*$^{fl/fl}$*;K14-Cre* mice. By SEM analysis, rugae formation was detectable in control mice, but not in their *Tgfbr2*$^{fl/fl}$*;K14-Cre* and *Tgfbr2*$^{fl/fl}$*;K14-Cre;Irf6*^{Tg} littermates (Fig. 5A-C). We also found that *Tgfbr2*$^{fl/fl}$*;K14-Cre* mice exhibit cleft soft palate, which was partially rescued (in the anterior of the soft palate) in *Tgfbr2*$^{fl/fl}$*;K14-Cre;Irf6*^{Tg} mice (Fig. 5B,C). In addition, *Tgfbr2*$^{fl/fl}$*;K14-Cre* mice have submucous cleft palate throughout the anterior to posterior regions of the hard palate, based on histology (Fig. 5K). At E15.5 and E16.5, the MEE disappeared in control mice, whereas MEE persistence was detectable in *Tgfbr2*$^{fl/fl}$*;K14-Cre* mice (Fig. 5D,E,G,H). *Tgfbr2*$^{fl/fl}$*;K14-Cre;Irf6*^{Tg} mice show a one-day delay in the disappearance of the MEE (Fig. 5F,I). In histological sections, we detected MEE persistence (*n*=14/14) corresponding with the groove in the midline of the palate in *Tgfbr2*$^{fl/fl}$*;K14-Cre* mice (Fig. 5K). Proper apoptotic degradation of the MEE was restored in *Tgfbr2*$^{fl/fl}$*;K14-Cre;Irf6*^{Tg} mice (*n*=7/7), based on histological analysis (Fig. 5L), indicating that TGFβ-mediated *Irf6* signaling is functionally important and sufficient for MEE disappearance.

IRF6 regulates MEE disappearance via p21 expression

Apoptosis is one of the ultimate fates of the MEE during palatal fusion (Cuervo and Covarrubias, 2004). Loss of *Tgfbr2* in the epithelium results in absence of apoptosis and maintenance of proliferation in MEE cells (Xu et al., 2006). We analyzed the cellular defect in persistent MEE cells by assaying both cell proliferation and apoptosis activities. We found that altered cell proliferation in the MEE was restored in *Tgfbr2*$^{fl/fl}$*;K14-Cre;Irf6*^{Tg} mice to a level comparable to the control (Fig. 6A-D). Similarly, we found that altered apoptotic activity in the MEE was also restored in *Tgfbr2*$^{fl/fl}$*;K14-Cre;Irf6*^{Tg} mice compared with the control (Fig. 6E-H). Thus, our data demonstrate that loss of *Tgfbr2* results in compromised *Irf6* expression, continuous cell proliferation, and failure of apoptosis in MEE cells, indicating that TGFβ-mediated *Irf6* expression plays a role in the disappearance of the MEE. We previously reported that *p21* (also known as *Cdkn1a*) was decreased in the MEE of *Tgfbr2*$^{fl/fl}$*;K14-Cre* mice (Xu et al., 2008). We hypothesized that *p21* expression might be regulated by the TGFβ-mediated IRF6 pathway. To investigate p21 expression, we performed immunohistochemical (Fig. 6I-K), immunoblotting

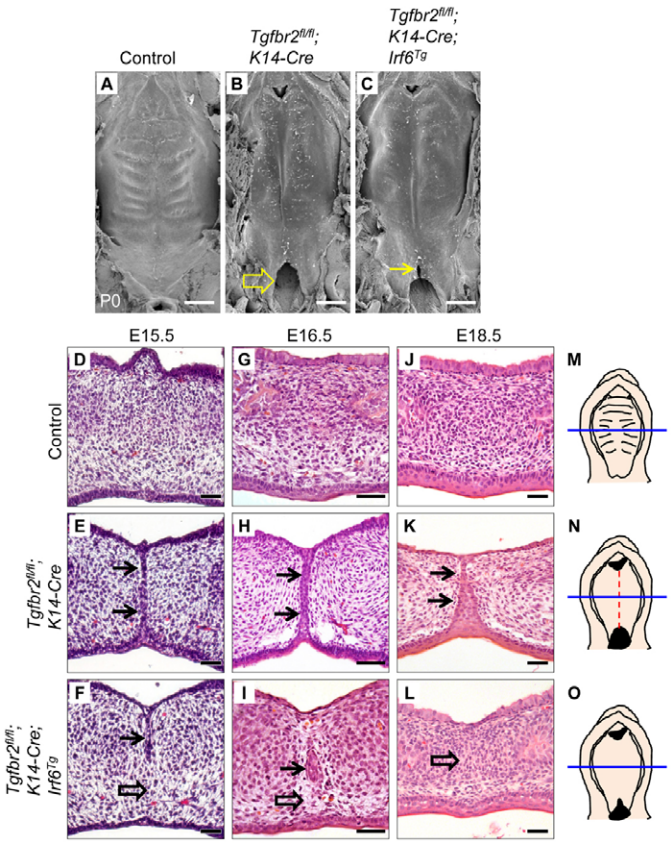

Fig. 5. Restored MEE degeneration in *Tgfbr2*$^{fl/fl}$*;K14-Cre* mice via overexpression of *Irf6*. (**A-C**) SEM images of the palates of newborn control (A), *Tgfbr2*$^{fl/fl}$*;K14-Cre* (B) and *Tgfbr2*$^{fl/fl}$*;K14-Cre;Irf6*^{Tg} (C) mice. Arrow in B indicates cleft soft palate. Arrow in C indicates a partial rescue of cleft soft palate in the anterior region of the soft palate. (**D-L**) H&E staining of E15.5 (D-F), E16.5 (G-I) and E18.5 (J-L) *Tgfbr2*$^{fl/fl}$ control, *Tgfbr2*$^{fl/fl}$*;K14-Cre* and *Tgfbr2*$^{fl/fl}$*;K14-Cre;Irf6*^{Tg} mice. Arrows indicate MEE persistence. Open arrows indicate MEE degeneration. The MEE was scored for persistence at E18.5: control mice, *n*=0/28; *Tgfbr2*$^{fl/fl}$*;K14-Cre* mice, *n*=14/14; *Tgfbr2*$^{fl/fl}$*;K14-Cre;Irf6*^{Tg} mice, *n*=0/7. (**M-O**) Schematics of E18.5 *Tgfbr2*$^{fl/fl}$ control (M), *Tgfbr2*$^{fl/fl}$*;K14-Cre* (N) and *Tgfbr2*$^{fl/fl}$*;K14-Cre;Irf6*^{Tg} (O) palates showing the position (blue lines, hard palate) from which the sections shown in D-L were taken. A dashed line (red, in N) indicates persistence of the MEE. Scale bars: 500 μm in A-C; 50 μm in D-L.

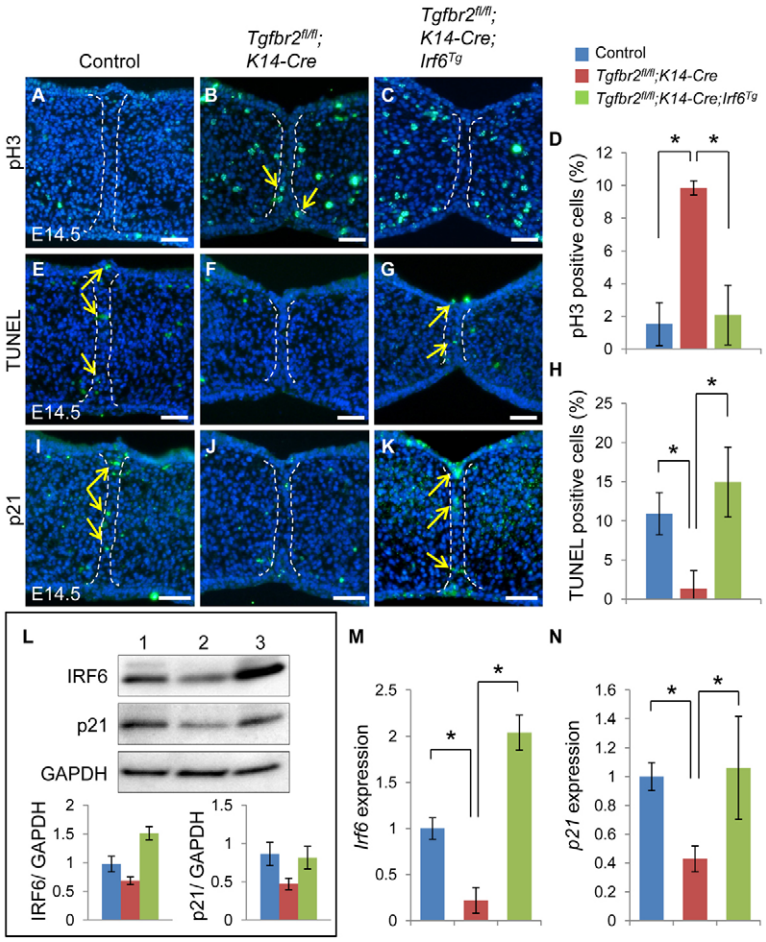

Fig. 6. p21 expression is restored in *Tgfbr2*$^{fl/fl}$*;K14-Cre;Irf6*^{Tg} mice. (**A-C**) Immunostaining of phosphorylated histone H3 (pH3) in *Tgfbr2*$^{fl/fl}$ control (A), *Tgfbr2*$^{fl/fl}$*;K14-Cre* (B) and *Tgfbr2*$^{fl/fl}$*;K14-Cre;Irf6*^{Tg} (C) mice at E14.5. Dashed lines indicate the MEE. Arrows indicate positive signal (green). (**D**) Percentage of pH3-positive nuclei in the palates of *Tgfbr2*$^{fl/fl}$ (blue bar, *n*=13), *Tgfbr2*$^{fl/fl}$*;K14-Cre* (red bar, *n*=7) and *Tgfbr2*$^{fl/fl}$*;K14-Cre;Irf6*^{Tg} (green bar, *n*=4) mice at E14.5. (**E-G**) TUNEL staining of *Tgfbr2*$^{fl/fl}$ control (E), *Tgfbr2*$^{fl/fl}$*;K14-Cre* (F) and *Tgfbr2*$^{fl/fl}$*;K14-Cre;Irf6*^{Tg} (G) mice at E14.5. Dashed lines indicate the MEE. Arrows indicate positive signal (green). (**H**) Percentage of TUNEL-labeled nuclei in the palates of *Tgfbr2*$^{fl/fl}$ (blue bar, *n*=13), *Tgfbr2*$^{fl/fl}$*;K14-Cre* (red bar, *n*=7) and *Tgfbr2*$^{fl/fl}$*;K14-Cre;Irf6*^{Tg} (green bar, *n*=4) mice at E14.5. (**I-K**) Immunohistochemical analyses of p21 expression in the palates of *Tgfbr2*$^{fl/fl}$ control (I), *Tgfbr2*$^{fl/fl}$*;K14-Cre* (J) and *Tgfbr2*$^{fl/fl}$*;K14-Cre;Irf6*^{Tg} (K) mice at E14.5. Dashed lines indicate the MEE. Arrows indicate positive signal (green). (**L**) Immunoblotting analysis of IRF6 and p21 in the MEE of *Tgfbr2*$^{fl/fl}$ control (lane 1), *Tgfbr2*$^{fl/fl}$*;K14-Cre* (lane 2) and *Tgfbr2*$^{fl/fl}$*;K14-Cre;Irf6*^{Tg} (lane 3) mice. GAPDH was used as a loading control. Bar graphs (below) show the ratio of IRF6 or p21 to GAPDH following quantitative densitometry analysis of immunoblotting data. *Tgfbr2*$^{fl/fl}$ control (blue bar), *Tgfbr2*$^{fl/fl}$*;K14-Cre* (red bar), *Tgfbr2*$^{fl/fl}$*;K14-Cre;Irf6*^{Tg} (green bar). Three samples were analyzed. (**M**,**N**) Quantitative RT-PCR analyses of *Irf6* (M) and *p21* (N) in the MEE of *Tgfbr2*$^{fl/fl}$ (blue, *n*=3), *Tgfbr2*$^{fl/fl}$*;K14-Cre* (red, *n*=3) and *Tgfbr2*$^{fl/fl}$*;K14-Cre;Irf6*^{Tg} (green, *n*=3) mice at E14.5. Error bars represent s.d. **P*<0.05. Scale bars: 50 μm.

(Fig. 6L) and quantitative RT-PCR (Fig. 6M,N) analyses. We found that p21 expression was restored in E14.5 *Tgfbr2*$^{fl/fl}$*;K14-Cre;Irf6*^{Tg} mice, correlating with *Irf6* expression. Therefore, we propose that TGFβ-mediated IRF6 activity regulates MEE disappearance by regulating p21 expression.

Previous studies have demonstrated that IRF6 induces degradation of the p63 isoform ΔNp63 and that this is linked with the pathogenesis of VWS and PPS (Moretti et al., 2010; Thomason et al., 2010). In addition, ΔNp63 represses transcription of *p21 in vitro* and *in vivo* (Laurikkala et al., 2006; Welsh and O'Brien, 2009; Westfall et al., 2003). Because there is no conserved IRF6-binding site in the promoter-proximal genomic region of *p21* (in at least six mammals, 5 kb upstream and 5 kb downstream of the TSS), we hypothesized that IRF6 might regulate *p21* expression via ΔNp63. ΔNp63 is only expressed in the basal epithelial layer during palate formation (Fakhouri et al., 2012). Indeed, increased ΔNp63 expression was detectable in basal epithelial cells in *Tgfbr2*$^{fl/fl}$*;K14-Cre* mice, consistent with a TGFβ-mediated IRF6/ΔNp63/p21 signaling cascade at E14.5 and E15.5 (Fig. 7A-F). Moreover, ΔNp63 expression was reversed by overexpression of *Irf6* (Fig. 7C,F). We also evaluated ΔNp63 expression levels in control, *Tgfbr2*$^{fl/fl}$*;K14-Cre* and *Tgfbr2*$^{fl/fl}$*;K14-Cre;Irf6*^{Tg} mice by immunoblotting (Fig. 7G). To confirm that *p21* expression is regulated by p63, we analyzed the mouse *p21* promoter region (2.5 kb upstream and 2.5 kb downstream of the TSS), and found two potential p63-binding sites in the mouse genomic region of *p21* (Fig. 7H). We performed ChIP analysis to test whether p63 could bind to the genomic region of *p21*, and found that the *p21* genomic region immunoprecipitated with the p63 antibody at p63-binding site 1 (+727 bp to +746 bp), but not at p63-binding site 2 (−436 bp to −455 bp) (Fig. 7I). These results indicate that *p21* expression is likely to be regulated through the TGFβ/IRF6/ΔNp63 signaling cascade.

Finally, we investigated the functional significance of the IRF6/p63/p21 signaling cascade using an *ex vivo* organ culture system. We found that either reduction of *p63* or overexpression of *p21* could restore the degeneration of the MEE (Fig. 8A-F). In addition, primary mouse keratinocytes were treated with *Tgfbr2*, *Irf6* or control siRNA (Fig. 8G). After siRNA knockdown for *Tgfbr2*, gene expression of *Irf6* and *p21* was significantly decreased and *p63* gene expression was significantly ($P<0.05$) upregulated. Similarly, *Irf6* siRNA knockdown resulted in downregulation of *Irf6* and *p21* gene expression and upregulation of *p63* gene expression. Previous studies indicate that *p63* expression is upregulated in E14.5 *Irf6*$^{R84C/R84C}$ palates (Thomason et al., 2010) and siRNA knockdown for *Irf6* results in upregulated p63 expression in human keratinocytes (Moretti et al., 2010). Therefore, we investigated whether p63 expression was altered in *Irf6*$^{R84C/R84C}$ palates. The expression of p63 was increased in *Irf6*$^{R84C/R84C}$ palates, consistent with previous findings (Fig. 8H,I). Collectively, these data suggest that *p21* expression is regulated through a TGFβ/IRF6/ΔNp63 signaling cascade (Fig. 8J).

DISCUSSION

Submucous cleft palate, which can result from MEE defects during palatal fusion, is one of the most common forms of cleft palate in

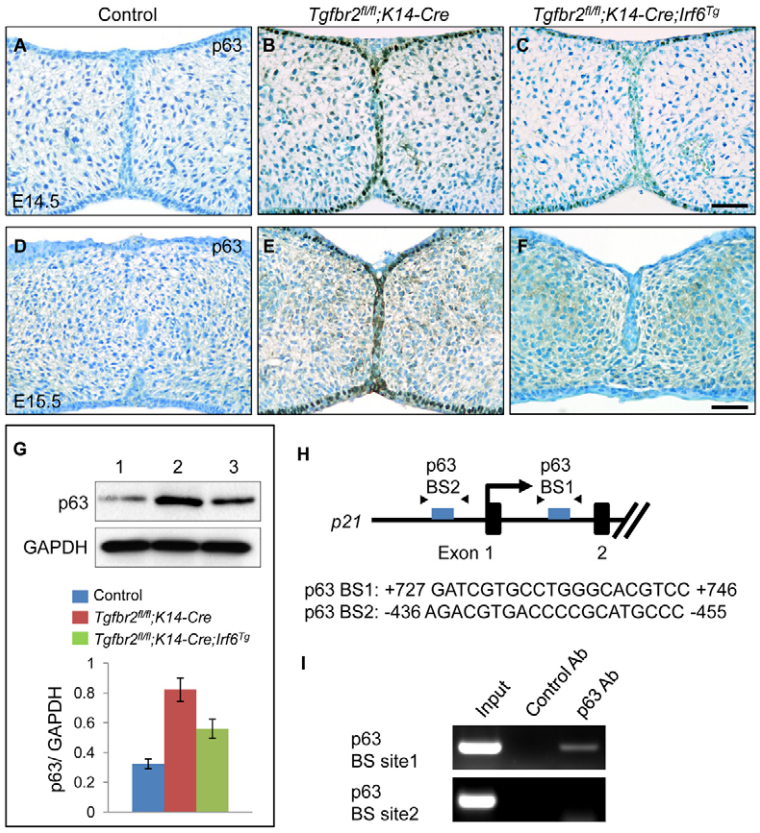

Fig. 7. Increased ΔNp63 expression in *Tgfbr2*$^{fl/fl}$*;K14-Cre* mice. (**A-F**) Immunohistochemical analyses of ΔNp63 expression in the palates of *Tgfbr2*$^{fl/fl}$ control (A,D), *Tgfbr2*$^{fl/fl}$*;K14-Cre* (B,E) and *Tgfbr2*$^{fl/fl}$*;K14-Cre;Irf6*^{Tg} (C,F) mice at E14.5 (A-C) and E15.5 (D-F). Brown, positive signal. Nuclei were counterstained with 0.03% Methylene Blue. Scale bars: 50 μm. (**G**) Immunoblotting analysis of p63 in the MEE of E14.5 *Tgfbr2*$^{fl/fl}$ control (lane 1), *Tgfbr2*$^{fl/fl}$*;K14-Cre* (lane 2) and *Tgfbr2*$^{fl/fl}$*;K14-Cre;Irf6*^{Tg} (lane 3) mice. GAPDH was used as a loading control. Bar graph (below) shows the ratio of p63 to GAPDH following quantitative densitometry analysis of immunoblotting data. Three samples were analyzed. (**H**) Schematic of the upstream region of the mouse *p21* gene (not to scale), showing locations of putative p63-binding sites tested in ChIP assays. Putative p63-binding sequences are shown below. Arrowheads indicate the position of primers used in ChIP analysis. (**I**) ChIP analysis of DNA fragments immunoprecipitated with a p63-specific antibody or with an isotype-specific control antibody. Immunoprecipitates were PCR amplified with primers flanking the putative p63-binding region. Input lane shows PCR amplification of the sonicated chromatin before immunoprecipitation. No amplification of target sites was detected when an isotype-specific control antibody was used. Ab, antibody; BS, binding site.

humans, but the molecular and developmental mechanism of submucous cleft palate are not well studied, in part because of the paucity of animal models that exhibit this phenotype (Funato et al., 2012; Pauws et al., 2009). MEE persistence affects palatal bone formation in the hard palate and muscle development in the soft palate; consequently, patients with submucous cleft palate need surgical and other procedures to develop precise physiological functions such as speech and swallowing.

We have generated an animal model in which loss of TGFβ signaling in MEE cells results in submucous cleft palate (Xu et al., 2006). In this study, we show that TGFβ-mediated *Irf6* expression is crucial for the fate of MEE cells. MEE degeneration in *Tgfbr2*$^{fl/fl}$*;K14-Cre* mice was restored by overexpression of *Irf6*, indicating that *Irf6* is functionally important for the MEE disappearance mediated by TGFβ signaling. Previous studies indicate that mice with loss of *Irf6* function exhibit cleft palate owing to failure of palatal shelf elevation resulting from adhesion between the palatal shelves and the tongue, following a defect in epithelial differentiation (Ingraham et al., 2006; Richardson et al., 2006). Because of the failure of palatal elevation in *Irf6*$^{R84C/R84C}$ mice, we were previously not able to investigate the role and function of *Irf6* during MEE disappearance fully. In this study, using an *ex vivo* organ culture system, we show for the first time that *Irf6*$^{R84C/R84C}$ mutation results in the absence of apoptosis and the maintenance of proliferation in the MEE, indicating that *Irf6* is crucial for MEE cell fate during palatal fusion. Although heterozygous *Irf6* mutant mice have normal palate formation, a combination of loss of *Smad4* and inhibition of p38 MAPK only led to ~50% reduction of *Irf6* expression and persistence of the MEE in *ex vivo* organ culture. This result suggests that there are other factors or signaling pathways that might regulate *Irf6* expression in addition to SMAD4/p38 MAPK signaling pathways (Ferretti et al., 2011; Letra et al., 2012). A recent study has shown that integration of IRF6 and the Notch ligand jagged 2 signaling is essential for controlling palatal adhesion and fusion during palatogenesis (Richardson et al., 2009). Interestingly, overexpression of *Irf6* in *Tgfbr2*$^{fl/fl}$*;K14-Cre* mice did not rescue the developmental defects in the palatal mesenchyme (supplementary material Fig. S5), suggesting that the TGFβ-mediated IRF6 signaling cascade plays a cell-autonomous role in regulating the fate of MEE cells during palatal fusion and that TGFβ regulates other downstream target genes that control the development of muscles in the soft palate through tissue-tissue interactions. Furthermore, using mutant mouse models, we found that TGFβ signaling regulates *Irf6* and *p21* expression and MEE disappearance via both SMAD-dependent and -independent pathways during palatal fusion.

SMAD4 mutations have been found in patients with unselected hereditary hemorrhagic telangiectasia (HHT), which is an autosomal dominant disease of vascular dysplasia (Gallione et al., 2006). The symptoms of HHT include epistaxis, telangiectases, and arteriovenous malformations, which are most often found in the lungs, brain, liver and gastrointestinal tract. In addition, *SMAD4* mutations have been identified in families with juvenile polyposis, aortophathy, and mitral valve dysfunction (Andrabi et al., 2011). Approximately 15% of people with juvenile polyposis syndrome have other abnormalities, such as cleft palate, polydactyly, intestinal malrotation, heart or brain abnormalities, and abnormalities of the genitalia or urinary tract. Although most *Smad4*$^{fl/fl}$*;K14*-Cre mice have normal palates, one copy of the R84C *IRF6* mutation in a *Smad4* mutant background (*Smad4*$^{fl/fl}$*;K14-Cre;Irf6*$^{+/R84C}$ mice) resulted in fully penetrant submucous cleft palate and polydactyly. It is important to note that *Smad4*$^{fl/fl}$*;K14-Cre;Irf6*$^{+/R84C}$ mice closely phenocopy individuals affected by PPS as described in

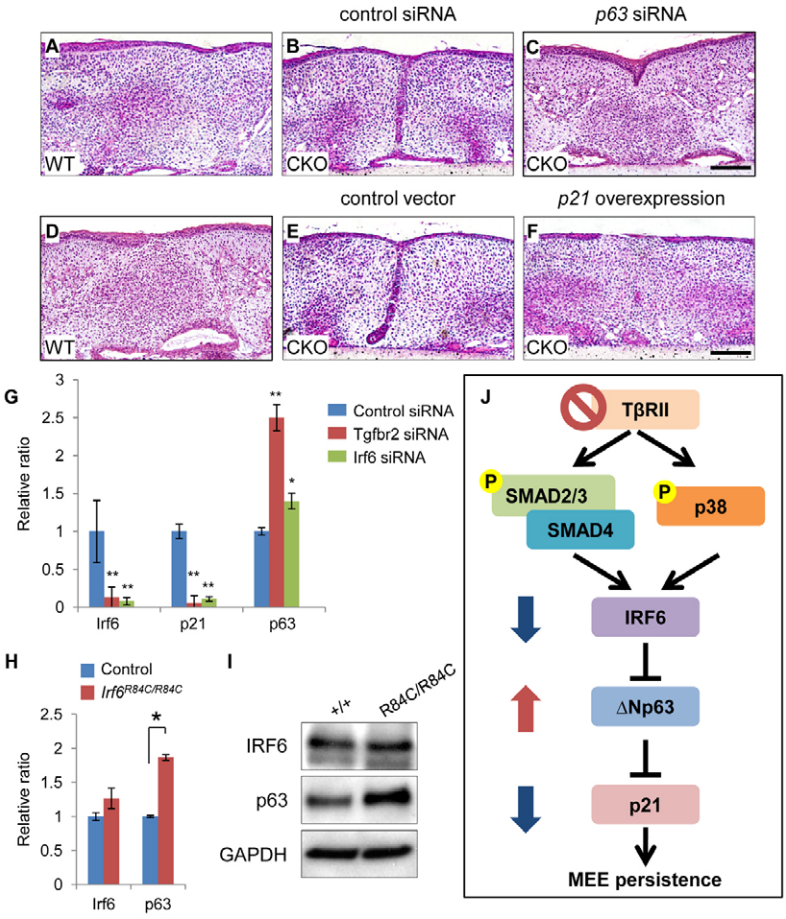

Fig. 8. Altered p63-p21 cascade results in persistence of the MEE in *Tgfbr2*$^{fl/fl}$;*K14-Cre* mice. (**A-C**) H&E staining of palate explants from *Tgfbr2*$^{fl/fl}$ (WT) mice and *Tgfbr2*$^{fl/fl}$;*K14-Cre* (CKO) mice treated with *p63* (C) or control (B) siRNA for 72 hours. *n*=5 per group. (**D-F**) H&E staining of palate explants from *Tgfbr2*$^{fl/fl}$ (WT) mice and *Tgfbr2*$^{fl/fl}$;*K14-Cre* (CKO) mice treated with *p21* overexpression vector (F) or control (E) for 72 hours. *n*=5 per group. (**G**) Quantitative RT-PCR analyses of *Irf6*, *p21* and *ΔNp63* expression in primary mouse keratinocytes isolated from back skin of newborn wild-type mice after treatment with control (blue bars), *Tgfbr2* (red bars) or *Irf6* (green bars) siRNA. Antisense siRNA was used as control. (**H**) Quantitative RT-PCR analyses of *Irf6* and *ΔNp63* expression in primary mouse keratinocytes isolated from newborn *Irf6*$^{R84C/R84C}$ (red bars) and littermate control (blue bars) back skin. (**I**) Immunoblotting analysis of IRF6 and p63 in the MEE of control (+/+) and *Irf6*$^{R84C/R84C}$ (R84C/R84C) mice. GAPDH was used as a loading control. (**J**) Schematic depicting our model of the mechanism of TGFβ-mediated *Irf6*-ΔNp63-*p21* gene regulation in *Tgfbr2*$^{fl/fl}$;*K14-Cre* palates. IRF6 expression is regulated through both SMAD and p38 MAPK pathways. In the absence of TGFβ receptor type II (TβRII), IRF6 expression decreases. ΔNp63 expression increases in the absence of TβRII resulting in reduced p21 expression in the palatal epithelium. Altered TGFβ-IRF6-ΔNp63-p21 activity results in the persistence of the MEE. P, phosphorylated. Error bars represent s.d. **P*<0.05; ***P*<0.01. Scale bars: 50 μm.

humans with *IRF6* mutation, whereas *Irf6*$^{+/R84C}$ mice do not show digit developmental defects. These results suggest that a compromised SMAD-dependent, TGFβ-mediated IRF6 signaling cascade might be responsible for developmental defects associated with PPS. Furthermore, an impaired TGFβ/IRF6 signaling cascade may cause submucosal cleft palate.

The secondary palate is divided into two parts: the anterior bony hard palate, which is about two-thirds of the secondary palate and is composed of bone, and the posterior fleshy soft palate, which is about one-third of the secondary palate and is composed of muscles. Our previous study suggests that loss of *Tgfbr2* in the epithelium causes cleft soft palate owing to failure of muscle development and misorientation of muscle fibers (Xu et al., 2006). Overexpression of *Irf6* in the MEE of *Tgfbr2*$^{fl/fl}$;*K14-Cre* mice failed to restore epithelial-mesenchymal interaction and to support soft palate muscle development. We are currently investigating the molecular and cellular mechanisms of soft palate muscle defects in *Tgfbr2*$^{fl/fl}$;*K14-Cre* mice.

Cleft soft palate in *Tgfbr2*$^{fl/fl}$;*K14-Cre* mice was not rescued in *Tgfbr2*$^{fl/fl}$;*K14-Cre*;*Irf6*^{Tg} mice. One possible explanation is that there are differential gene expression patterns in the anterior versus the posterior in the MEE. Expression of *Irf6*, *p63* and *Tgfb3* is detectable throughout the oral epithelia in wild-type mice with no variation along the antero-posterior axis of the secondary palate (Fakhouri et al., 2012; Richardson et al., 2009; Yang et al., 2008). However, gene expression of *Tgfb3* was compromised specifically in the posterior palate in *Irf6*$^{R84C/R84C}$ mice, indicating that *Tgfb3* expression is differentially regulated between the anterior and posterior MEE (Richardson et al., 2009). It also suggests that IRF6 provides a feedback in regulating TGFβ signaling in the posterior region of developing palate.

WNT/β-catenin signaling acts upstream of *Irf6* in the lip epithelium during lip fusion (Ferretti et al., 2011). A previous study has shown that loss of WNT/β-catenin signaling results in downregulation of TGFβ, whereas expression of stabilized β-catenin in the palatal epithelium can cause ectopic *Tgfb3* expression and fusion of the palatal shelf and mandible (He et al., 2011). This study clearly demonstrates that a precisely controlled TGFβ signaling level is crucial for regulating the fate of MEE cells during palatal fusion. Ablation of *p63* results in diminished *Irf6* expression in the palate (Moretti et al., 2010; Thomason et al., 2010), and IRF6 can regulate ΔNp63 degradation in human keratinocytes (Moretti et al., 2010). However, we found that upregulated *p63* expression in wild-type mice did not affect the expression of *Irf6* in MEE cells (data not shown), indicating that there is no apparent feedback loop from upregulated p63 to *Irf6* expression.

In summary, our data indicate that a combination of genetic mutations in *Irf6* and *Smad4* cause submucous cleft palate and that TGFβ-mediated IRF6 activity is crucial for MEE disappearance. This is a significant advancement in our understanding of the mechanism of TGFβ signaling-associated cleft palate. Our findings that TGFβ-mediated *Irf6* expression is responsible for MEE disappearance and that overexpression of *Irf6* normalizes MEE cell fate determination in *Tgfbr2*$^{fl/fl}$;*K14-Cre* mice might provide potential therapeutic approaches for individuals with altered TGFβ signaling and submucous cleft palate. In addition, we propose that combined mutations in *IRF6* and *SMAD4* in humans might be useful diagnostic biomarkers for patients with cleft palate.

Acknowledgements
We are grateful to Dr Julie Mayo for critical reading of the manuscript, and to Dr Harold Slavkin for discussion. We thank Dr Harold Moses for *Tgfbr2*$^{fl/fl}$ mice. We thank Xuemei Deng, Toshiaki Yokota, Pablo Bringas Jr. and the Molecular Imaging Center and Center for Electron Microscopy and Microanalysis of USC for technical assistance.

Funding
This study was supported by grants from the National Institutes of Health National Institute of Dental and Craniofacial Research [DE020065 and DE012711 to Y.C,]; and from the UK Medical Research Council [G0901539 to M.J.D.]. Deposited in PMC for release after 6 months.

Competing interests statement
The authors declare no competing financial interests.

Supplementary material
Supplementary material available online at
http://dev.biologists.org/lookup/suppl/doi:10.1242/dev.089615/-/DC1

References

Andrabi, S., Bekheirnia, M. R., Robbins-Furman, P., Lewis, R. A., Prior, T. W. and Potocki, L. (2011). SMAD4 mutation segregating in a family with juvenile polyposis, aortopathy, and mitral valve dysfunction. *Am. J. Med. Genet. A.* **155**, 1165-1169.
Black, B. L. and Olson, E. N. (1998). Transcriptional control of muscle development by myocyte enhancer factor-2 (MEF2) proteins. *Annu. Rev. Cell Dev. Biol.* **14**, 167-196.
Cai, B. H., Chao, C. F., Lu, M. H., Lin, H. C. and Chen, J. Y. (2012). A half-site of the p53-binding site on the keratin 14 promoter is specifically activated by p63. *J. Biochem.* **152**, 99-110.
Chen, R. H., Su, Y. H., Chuang, R. L. and Chang, T. Y. (1998). Suppression of transforming growth factor-beta-induced apoptosis through a phosphatidylinositol 3-kinase/Akt-dependent pathway. *Oncogene* **17**, 1959-1968.
Cuervo, R. and Covarrubias, L. (2004). Death is the major fate of medial edge epithelial cells and the cause of basal lamina degradation during palatogenesis. *Development* **131**, 15-24.
Denissova, N. G., Pouponnot, C., Long, J., He, D. and Liu, F. (2000). Transforming growth factor beta -inducible independent binding of SMAD to the Smad7 promoter. *Proc. Natl. Acad. Sci. USA* **97**, 6397-6402.
Dixon, M. J., Marazita, M. L., Beaty, T. H. and Murray, J. C. (2011). Cleft lip and palate: understanding genetic and environmental influences. *Nat. Rev. Genet.* **12**, 167-178.
el-Deiry, W. S., Kern, S. E., Pietenpol, J. A., Kinzler, K. W. and Vogelstein, B. (1992). Definition of a consensus binding site for p53. *Nat. Genet.* **1**, 45-49.
Fakhouri, W. D., Rhea, L., Du, T., Sweezer, E., Morrison, H., Fitzpatrick, D., Yang, B., Dunnwald, M. and Schutte, B. C. (2012). MCS9.7 enhancer activity is highly, but not completely, associated with expression of Irf6 and p63. *Dev. Dyn.* **241**, 340-349.
Ferretti, E., Li, B., Zewdu, R., Wells, V., Hebert, J. M., Karner, C., Anderson, M. J., Williams, T., Dixon, J., Dixon, M. J. et al. (2011). A conserved Pbx-Wnt-p63-Irf6 regulatory module controls face morphogenesis by promoting epithelial apoptosis. *Dev. Cell* **21**, 627-641.
Fujii, Y., Shimizu, T., Kusumoto, M., Kyogoku, Y., Taniguchi, T. and Hakoshima, T. (1999). Crystal structure of an IRF-DNA complex reveals novel DNA recognition and cooperative binding to a tandem repeat of core sequences. *EMBO J.* **18**, 5028-5041.
Funato, N., Nakamura, M., Richardson, J. A., Srivastava, D. and Yanagisawa, H. (2012). Tbx1 regulates oral epithelial adhesion and palatal development. *Hum. Mol. Genet.* **21**, 2524-2537.
Gallione, C. J., Richards, J. A., Letteboer, T. G., Rushlow, D., Prigoda, N. L., Leedom, T. P., Ganguly, A., Castells, A., Ploos van Amstel, J. K., Westermann, C. J. et al. (2006). SMAD4 mutations found in unselected HHT patients. *J. Med. Genet.* **43**, 793-797.
Giehl, K., Seidel, B., Gierschik, P., Adler, G. and Menke, A. (2000). TGFbeta1 represses proliferation of pancreatic carcinoma cells which correlates with Smad4-independent inhibition of ERK activation. *Oncogene* **19**, 4531-4541.
Han, J. and Molkentin, J. D. (2000). Regulation of MEF2 by p38 MAPK and its implication in cardiomyocyte biology. *Trends Cardiovasc. Med.* **10**, 19-22.
He, F., Xiong, W., Wang, Y., Li, L., Liu, C., Yamagami, T., Taketo, M. M., Zhou, C. and Chen, Y. (2011). Epithelial Wnt/β-catenin signaling regulates palatal shelf fusion through regulation of Tgfβ3 expression. *Dev. Biol.* **350**, 511-519.
Hocevar, B. A., Brown, T. L. and Howe, P. H. (1999). TGF-beta induces fibronectin synthesis through a c-Jun N-terminal kinase-dependent, Smad4-independent pathway. *EMBO J.* **18**, 1345-1356.
Hu, P. P., Shen, X., Huang, D., Liu, Y., Counter, C. and Wang, X. F. (1999). The MEK pathway is required for stimulation of p21(WAF1/CIP1) by transforming growth factor-beta. *J. Biol. Chem.* **274**, 35381-35387.
Ingraham, C. R., Kinoshita, A., Kondo, S., Yang, B., Sajan, S., Trout, K. J., Malik, M. I., Dunnwald, M., Goudy, S. L., Lovett, M. et al. (2006). Abnormal skin, limb and craniofacial morphogenesis in mice deficient for interferon regulatory factor 6 (Irf6). *Nat. Genet.* **38**, 1335-1340.
Ito, Y., Yeo, J. Y., Chytil, A., Han, J., Bringas, P., Jr, Nakajima, A., Shuler, C. F., Moses, H. L. and Chai, Y. (2003). Conditional inactivation of Tgfbr2 in cranial neural crest causes cleft palate and calvaria defects. *Development* **130**, 5269-5280.
Iwata, J., Ezaki, J., Komatsu, M., Yokota, S., Ueno, T., Tanida, I., Chiba, T., Tanaka, K. and Kominami, E. (2006). Excess peroxisomes are degraded by autophagic machinery in mammals. *J. Biol. Chem.* **281**, 4035-4041.
Iwata, J., Hosokawa, R., Sanchez-Lara, P. A., Urata, M., Slavkin, H. and Chai, Y. (2010). Transforming growth factor-beta regulates basal transcriptional regulatory machinery to control cell proliferation and differentiation in cranial neural crest-derived osteoprogenitor cells. *J. Biol. Chem.* **285**, 4975-4982.
Iwata, J., Parada, C. and Chai, Y. (2011). The mechanism of TGF-β signaling during palate development. *Oral Dis.* **17**, 733-744.
Iwata, J., Hacia, J. G., Suzuki, A., Sanchez-Lara, P. A., Urata, M. and Chai, Y. (2012). Modulation of noncanonical TGF-β signaling prevents cleft palate in Tgfbr2 mutant mice. *J. Clin. Invest.* **122**, 873-885.
Kang, J. S., Liu, C. and Derynck, R. (2009). New regulatory mechanisms of TGF-beta receptor function. *Trends Cell Biol.* **19**, 385-394.
Koillinen, H., Lahermo, P., Rautio, J., Hukki, J., Peyrard-Janvid, M. and Kere, J. (2005). A genome-wide scan of non-syndromic cleft palate only (CPO) in Finnish multiplex families. *J. Med. Genet.* **42**, 177-184.
Kondo, S., Schutte, B. C., Richardson, R. J., Bjork, B. C., Knight, A. S., Watanabe, Y., Howard, E., de Lima, R. L., Daack-Hirsch, S., Sander, A. et al. (2002). Mutations in IRF6 cause Van der Woude and popliteal pterygium syndromes. *Nat. Genet.* **32**, 285-289.
Kouwenhoven, E. N., van Heeringen, S. J., Tena, J. J., Oti, M., Dutilh, B. E., Alonso, M. E., de la Calle-Mustienes, E., Smeenk, L., Rinne, T., Parsaulian, L. et al. (2010). Genome-wide profiling of p63 DNA-binding sites identifies an element that regulates gene expression during limb development in the 7q21 SHFM1 locus. *PLoS Genet.* **6**, e1001065.
Larkin, M. A., Blackshields, G., Brown, N. P., Chenna, R., McGettigan, P. A., McWilliam, H., Valentin, F., Wallace, I. M., Wilm, A., Lopez, R. et al. (2007). Clustal W and Clustal X version 2.0. *Bioinformatics* **23**, 2947-2948.
Laurikkala, J., Mikkola, M. L., James, M., Tummers, M., Mills, A. A. and Thesleff, I. (2006). p63 regulates multiple signalling pathways required for ectodermal organogenesis and differentiation. *Development* **133**, 1553-1563.
Letra, A., Fakhouri, W., Fonseca, R. F., Menezes, R., Kempa, I., Prasad, J. L., McHenry, T. G., Lidral, A. C., Moreno, L., Murray, J. C. et al. (2012). Interaction between IRF6 and TGFA genes contribute to the risk of nonsyndromic cleft lip/palate. *PLoS ONE* **7**, e45441.
Little, H. J., Rorick, N. K., Su, L. I., Baldock, C., Malhotra, S., Jowitt, T., Gakhar, L., Subramanian, R., Schutte, B. C., Dixon, M. J. et al. (2009). Missense mutations that cause Van der Woude syndrome and popliteal pterygium syndrome affect the DNA-binding and transcriptional activation functions of IRF6. *Hum. Mol. Genet.* **18**, 535-545.
Massagué, J. (2012). TGFβ signalling in context. *Nat. Rev. Mol. Cell Biol.* **13**, 616-630.
Moretti, F., Marinari, B., Lo Iacono, N., Botti, E., Giunta, A., Spallone, G., Garaffo, G., Vernersson-Lindahl, E., Merlo, G., Mills, A. A. et al. (2010). A regulatory feedback loop involving p63 and IRF6 links the pathogenesis of 2 genetically different human ectodermal dysplasias. *J. Clin. Invest.* **120**, 1570-1577.
Mossey, P. A., Little, J., Munger, R. G., Dixon, M. J. and Shaw, W. C. (2009). Cleft lip and palate. *Lancet* **374**, 1773-1785.
Pauws, E., Hoshino, A., Bentley, L., Prajapati, S., Keller, C., Hammond, P., Martinez-Barbera, J. P., Moore, G. E. and Stanier, P. (2009). Tbx22null mice have a submucous cleft palate due to reduced palatal bone formation and also display ankyloglossia and choanal atresia phenotypes. *Hum. Mol. Genet.* **18**, 4171-4179.
Perez, C. A., Ott, J., Mays, D. J. and Pietenpol, J. A. (2007). p63 consensus DNA-binding site: identification, analysis and application into a p63MH algorithm. *Oncogene* **26**, 7363-7370.
Richardson, R. J., Dixon, J., Malhotra, S., Hardman, M. J., Knowles, L., Boot-Handford, R. P., Shore, P., Whitmarsh, A. and Dixon, M. J. (2006). Irf6 is a key determinant of the keratinocyte proliferation-differentiation switch. *Nat. Genet.* **38**, 1329-1334.
Richardson, R. J., Dixon, J., Jiang, R. and Dixon, M. J. (2009). Integration of IRF6 and Jagged2 signalling is essential for controlling palatal adhesion and fusion competence. *Hum. Mol. Genet.* **18**, 2632-2642.
Ross, S. and Hill, C. S. (2008). How the Smads regulate transcription. *Int. J. Biochem. Cell Biol.* **40**, 383-408.
Schmierer, B. and Hill, C. S. (2007). TGFbeta-SMAD signal transduction: molecular specificity and functional flexibility. *Nat. Rev. Mol. Cell Biol.* **8**, 970-982.

Shi, Y. and Massagué, J. (2003). Mechanisms of TGF-beta signaling from cell membrane to the nucleus. *Cell* **113**, 685-700.
Sorrentino, A., Thakur, N., Grimsby, S., Marcusson, A., von Bulow, V., Schuster, N., Zhang, S., Heldin, C. H. and Landström, M. (2008). The type I TGF-beta receptor engages TRAF6 to activate TAK1 in a receptor kinase-independent manner. *Nat. Cell Biol.* **10**, 1199-1207.
Srichomthong, C., Siriwan, P. and Shotelersuk, V. (2005). Significant association between IRF6 820G->A and non-syndromic cleft lip with or without cleft palate in the Thai population. *J. Med. Genet.* **42**, e46.
Thomason, H. A., Zhou, H., Kouwenhoven, E. N., Dotto, G. P., Restivo, G., Nguyen, B. C., Little, H., Dixon, M. J., van Bokhoven, H. and Dixon, J. (2010). Cooperation between the transcription factors p63 and IRF6 is essential to prevent cleft palate in mice. *J. Clin. Invest.* **120**, 1561-1569.
Toro, R., Saadi, I., Kuburas, A., Nemer, M. and Russo, A. F. (2004). Cell-specific activation of the atrial natriuretic factor promoter by PITX2 and MEF2A. *J. Biol. Chem.* **279**, 52087-52094.
Welsh, I. C. and O'Brien, T. P. (2009). Signaling integration in the rugae growth zone directs sequential SHH signaling center formation during the rostral outgrowth of the palate. *Dev. Biol.* **336**, 53-67.
Westfall, M. D., Mays, D. J., Sniezek, J. C. and Pietenpol, J. A. (2003). The Delta Np63 alpha phosphoprotein binds the p21 and 14-3-3 sigma promoters in vivo and has transcriptional repressor activity that is reduced by Hay-Wells syndrome-derived mutations. *Mol. Cell. Biol.* **23**, 2264-2276.
Wong, F. K. and Hagg, U. (2004). An update on the aetiology of orofacial clefts. *Hong Kong Med. J.* **10**, 331-336.
Xu, X., Han, J., Ito, Y., Bringas, P., Jr, Urata, M. M. and Chai, Y. (2006). Cell autonomous requirement for Tgfbr2 in the disappearance of medial edge epithelium during palatal fusion. *Dev. Biol.* **297**, 238-248.
Xu, X., Han, J., Ito, Y., Bringas, P., Jr, Deng, C. and Chai, Y. (2008). Ectodermal Smad4 and p38 MAPK are functionally redundant in mediating TGF-beta/BMP signaling during tooth and palate development. *Dev. Cell* **15**, 322-329.
Yamashita, M., Fatyol, K., Jin, C., Wang, X., Liu, Z. and Zhang, Y. E. (2008). TRAF6 mediates Smad-independent activation of JNK and p38 by TGF-beta. *Mol. Cell* **31**, 918-924.
Yang, L. T., Li, W. Y. and Kaartinen, V. (2008). Tissue-specific expression of Cre recombinase from the Tgfb3 locus. *Genesis* **46**, 112-118.
Zawel, L., Dai, J. L., Buckhaults, P., Zhou, S., Kinzler, K. W., Vogelstein, B. and Kern, S. E. (1998). Human Smad3 and Smad4 are sequence-specific transcription activators. *Mol. Cell* **1**, 611-617.
Zhang, Y. E. (2009). Non-Smad pathways in TGF-beta signaling. *Cell Res.* **19**, 128-139.